

The right top coupling in the aligned two-Higgs-doublet model

Cesar Ayala^{*1,2}, Gabriel A. González-Sprinberg^{†3}, R. Martínez^{‡4} and Jordi Vidal^{§1}

¹*Departament de Física Teòrica, Universitat de València & Instituto de Física Corpuscular (IFIC), Centro Mixto Universitat de València-CSIC, E-46100 Burjassot, València, Spain.*

²*Department of Physics, Universidad Técnica Federico Santa María, Casilla 110-V, Valparaíso, Chile.*

³*Instituto de Física, Facultad de Ciencias, Universidad de la República, Igúá 4225, Montevideo 11600, Uruguay.*

⁴*Departamento de Física, Universidad Nacional de Colombia, Bogotá Distrito Capital, Colombia*

October 31, 2018

Abstract

We compute the right top quark coupling in the aligned two-Higgs-doublet model. In the Standard Model the real part of this coupling is dominated by QCD-gluon-exchange diagram, but the imaginary part, instead, is purely electroweak at one loop. Within this model we show that values for the imaginary part of the coupling up to one order of magnitude larger than the electroweak prediction can be obtained. For the real part of the electroweak contribution we find that it can be up to three orders of magnitude larger than the standard model one. We also present detailed results of the one loop analytical computation.

1 Introduction

In 2015 the LHC center-of-mass energy has reached 13 TeV. By the end of 2016 the LHC will be close to a peak luminosity of $1.5 \times 10^{34} \text{ cm}^{-2} \text{ s}^{-1}$, with an integrated luminosity of 38 fb^{-1} . After 2020, several components of the accelerator will reach

*cesar.ayala@uv.es

†gabrielg@fisica.edu.uy

‡remartinezm@unal.edu.co

§vidal@uv.es

the radiation damage or reliability limit so that, by 2024 the LHC will have to be upgraded to the High-Luminosity LHC (HL-LHC), which is expected to accumulate over the next 10 years an impressive integrated luminosity of 3000 fb^{-1} at energies close to 13-14 TeV [1, 2]. The CMS and Atlas experiments have already collected millions of top quark pairs and single top events but in this scenario of very high luminosity, they will detect billions of them in the future. Besides, next generation of colliders, such as CLIC, will eventually be built and it is expected that the top quarks physics will enter in an era of high precision. The top quark is the only quark that decays weakly before hadronization and, up to now, only one decay mode, $t \rightarrow bW^+$, is known. It was detected for the first time at TEVATRON [3, 4] where many of its physical properties were first measured and also some limits on the anomalous tbW couplings were set [5–7].

Top quark physics is considered as one of the gateways to new physics [8–10] and the study of its decay properties at the LHC [11–14] is being extensively investigated by the ATLAS and CMS collaborations [15, 16]. The determination of other couplings of the top quark, such as the chromoelectric and chromomagnetic of the ttg (top-top-gluon) vertex has been recently suggested [17] as a window for new physics, in the two-Higgs-doublet model ($2HDM$) framework with a CP -violating potential. The study of the different helicity components of the W in the top decay has been also proposed to investigate the tbW Lorentz vertex structure [18]. In recent works [19–24] it has been shown that a precise determination of the Lorentz form factors of the tbW vertex can be done with a suitable choice of observables built from longitudinal and transverse helicities of the W coming from the top decay.

The enormous amount of collected data by the LHC (and in the future by the HL-LHC) will determine the complete structure of the tWb vertex, with a precise determination of the properties of top quark couplings to the W boson and to the b quark.

The most general parametrization of the on-shell vertex needs four couplings. In the Standard Model (SM) the left coupling V_L is not zero and takes a value close to one [25]. The other three are zero at tree level: the chiral V_R coupling, and the left g_L and right g_R anomalous tensorial couplings. This is not the case in extended models where, in addition, some of these couplings can also be sensitive to new CP -violation mechanisms. The measurement of the two tensorial couplings $g_{L,R}$ at the LHC was investigated in ref. [26]. The values of $g_{L,R}$ within the SM, the $2HDM$ and other extended models were recently calculated in refs. [27–29] and they will not be considered in this paper. The right top coupling V_R was computed in the SM at leading order in ref. [30].

The LHC observables considered in the literature are not, in general, very sensitive to the right coupling V_R . This is due to the fact that in the lagrangian the V_R coupling has the same parity and chirality properties than the leading coupling V_L , so that the observables receive contributions from both terms. Some of these observables are the angular asymmetries in the W rest frame [18, 19, 31, 32], angular asymmetries in the top rest frame [19, 32–34] and spin correlations [19, 32, 35, 36]. In ref. [30] some of these observables were redefined in order to be directly proportional to the coupling we are interested in, V_R , in such a way as to cancel the leading V_L contribution to them. Then, these observables are directly sensitive to V_R and can be an important tool in order to

search for new physics contributions to this coupling.

A simple and widely studied extension of the electroweak theory is to consider a second scalar doublet added to the SM. However, tree level flavour changing neutral currents (FCNC) arise unless new hypothesis are introduced. A solution to this issue is the aligned two Higgs doublet model $A2HDM$ [37], where the two Yukawa matrices coupled to the same type of right-handed fermion are aligned in flavour space. Then, no FCNCs appear at tree level. Besides, most of the popular versions of the $2HDM$ are reproduced with particular choices of the $A2HDM$ parameters. In this paper we present a detailed calculation of the new contributions to the V_R top right coupling in the general framework of the $A2HDM$.

This work is organized as follows. In the next section we briefly review the $A2HDM$, introducing the notation used in the paper and presenting the current limits that constraint the parameters of the model. In section 3 we define the vertex parametrization and show the details of the computation of the different contributions to the right vector coupling V_R within the $A2HDM$. In section 4 we investigate the sensitivity of the V_R coupling to the scalar mixing angle and alignments parameters, for a CP-conserving scalar potential. We show the results obtained for values of the parameters of the model and masses of the new particles so as to cover the meaningful parameter space of the model. The results for $2HDM$ Type-I and II are also shown. We present our conclusions in section 5.

2 The aligned two-Higgs-doublet model

The $2HDM$ extends the SM by adding a second scalar doublet $\phi_2(x)$ with the same hypercharge $Y = 1/2$ [38, 39]. Similarly to what happens in the SM, after symmetry breaking, the neutral components of the two doublets get non zero vacuum expectation values $\langle \phi_i \rangle_{i=1,2}^T = (0, \frac{v_i}{\sqrt{2}} e^{i\theta_i})$.

The so called Higgs basis $(\Phi_1(x), \Phi_2(x))$ is obtained through a rotation of the $\phi_1(x), \phi_2(x)$ states given by the angle β (defined as $\tan \beta = \frac{v_2}{v_1}$), in such a way that only one of the doublets ($\Phi_1(x)$) gets a non-zero expectation value $v = \sqrt{v_1^2 + v_2^2}$.

In this basis, the three components of the doublets can be written as

$$\Phi_1(x) = \begin{pmatrix} G^+(x) \\ \frac{1}{\sqrt{2}}(v + S_1(x) + iG^0(x)) \end{pmatrix}, \quad \Phi_2(x) = \begin{pmatrix} H^+(x) \\ \frac{1}{\sqrt{2}}(S_2(x) + iS_3(x)) \end{pmatrix} \quad (1)$$

where $G^0(x)$ and $G^\pm(x)$ correspond to the three would-be Goldstone bosons of the SM, $H^\pm(x)$ are two new charged scalar fields and $\{S_i(x)\}_{i=1,2,3}$ are three neutral scalars with no defined mass. To get the three mass eigenstates as a linear combination of the later three scalars one has to perform an orthogonal transformation \mathcal{R} so that the new three mass eigenstates, $\{\varphi_i(x)\}_{i=1,2,3} = \{h(x), H(x), A(x)\}$, can be written as

$$\varphi_i(x) = \mathcal{R}_{ij} S_j(x); \quad i, j = 1, 2, 3. \quad (2)$$

The particular form of the potential will define the matrix \mathcal{R} and the structure of the scalar mass matrix and mass eigenstates. If the potential is CP-conserving, the

CP-even states $\{S_1(x), S_2(x)\}$ will not mix with the CP-odd one ($S_3(x)$) so that:

$$\begin{aligned} H(x) &= \cos \gamma S_1(x) + \sin \gamma S_2(x) \\ h(x) &= -\sin \gamma S_1(x) + \cos \gamma S_2(x) \\ A(x) &= S_3(x) \end{aligned} \quad (3)$$

where γ is the neutral scalars mixing angle.

The most general Yukawa Lagrangian, with standard fermionic content will have different couplings to $\Phi_1(x)$ and $\Phi_2(x)$ doublets. It means that when one diagonalizes the fermionic mass matrices -in the Higgs basis- this transformation will not diagonalize the fermion-scalar Yukawa matrices. The Yukawa lagrangian can then be written as

$$\begin{aligned} \mathcal{L}_Y &= -\frac{\sqrt{2}}{v} \left\{ \bar{Q}_L(x) [\mathcal{M}_d \Phi_1(x) + \mathcal{Y}_d \Phi_2(x)] d'_R(x) \right. \\ &\quad + \bar{Q}_L(x) [\mathcal{M}_u \tilde{\Phi}_1(x) + \mathcal{Y}_u \tilde{\Phi}_2(x)] u'_R(x) \\ &\quad \left. + \bar{L}_L(x) [\mathcal{M}_l \Phi_1(x) + \mathcal{Y}_l \Phi_2(x)] l'_R(x) + h.c. \right\}, \end{aligned} \quad (4)$$

where $\tilde{\Phi}_i(x) = i\tau_2 \Phi_i^*(x)$, all fermionic fields, $Q_L(x)$, $L_L(x)$, $d'_R(x)$, $u'_R(x)$ and $l'_R(x)$, are three-dimensional vectors in the flavour space, \mathcal{M}_f ($f = d, u, l$) are the non-diagonal 3×3 fermion mass matrices, and \mathcal{Y}_f are the fermion-scalar Yukawa couplings that are, in general, also non-diagonal. The rotation to the fermionic mass eigenstates ($d(x)$, $u(x)$, $l(x)$, $\nu(x)$) which diagonalizes the mass matrices \mathcal{M}_f will, in general, not diagonalize simultaneously the Yukawa matrices \mathcal{Y}_f , so that they will introduce FCNC at tree level. Among the different approaches to avoid this unwanted effect we choose the one that, before diagonalization, makes both Yukawa matrices - \mathcal{M}_f and \mathcal{Y}_f , for each type of right handed fermions- proportional to each other (alignment in the flavour space). Then, they can be simultaneously diagonalized and the diagonal Yukawa matrices satisfy the relations:

$$Y_j = \varsigma_j M_j, \quad i = d, l \quad Y_u = \varsigma_u M_u, \quad \varsigma_f^* = \frac{\xi_f - \tan \beta}{1 + \xi_f \tan \beta}, \quad f = u, d, l \quad (5)$$

with ξ_f being an arbitrary complex number and M_f ($f \equiv u, d, l$) diagonal mass matrices. This is the so called $A2HDM$. It has the advantage that for different values of the ξ_f parameter (see [37]) it reproduces the $2HDM$ with discrete Z_2 symmetries, Type-I, II, X, Y and inert model. Obviously if the ς_f are taken to be arbitrary complex numbers the Lagrangian incorporate new sources of CP-violation.

The Yukawa lagrangian can be then written as:

$$\begin{aligned} \mathcal{L}_Y &= -\frac{\sqrt{2}}{v} H^+(x) \bar{u}(x) [\varsigma_d V M_d P_R - \varsigma_u M_u V P_L] d(x) \\ &\quad -\frac{\sqrt{2}}{v} H^+(x) \varsigma_l \bar{\nu}(x) M_l P_R l(x) \\ &\quad -\frac{1}{v} \sum_{i,f} \varphi_i(x) y_f^{\varphi_i} \bar{f}(x) M_f P_R f(x) + h.c. , \end{aligned} \quad (6)$$

where V is the Cabibbo-Kobayashi-Maskawa matrix and $P_{R,L} \equiv \frac{1}{2}(1 \pm \gamma_5)$ are the chirality projectors.

The neutral Yukawa terms are flavor-diagonal and the couplings $y_f^{\varphi_i}$ ($\varphi_i = h, H, A$) are proportional to the corresponding elements of the neutral scalar mixing matrix \mathcal{R} :

$$\begin{aligned} y_{d,l}^{\varphi_i} &= \mathcal{R}_{i1} + (\mathcal{R}_{i2} + i\mathcal{R}_{i3}) \varsigma_{d,l}, \\ y_u^{\varphi_i} &= \mathcal{R}_{i1} + (\mathcal{R}_{i2} - i\mathcal{R}_{i3}) \varsigma_u^* \end{aligned} \quad (7)$$

that, in the particular case of a CP-conserving potential can be written as:

$$\begin{aligned} y_{d,l}^H &= \cos \gamma + \sin \gamma \varsigma_{d,l}, & y_u^H &= \cos \gamma + \sin \gamma \varsigma_u^*, \\ y_{d,l}^h &= -\sin \gamma + \cos \gamma \varsigma_{d,l}, & y_u^h &= -\sin \gamma + \cos \gamma \varsigma_u^*, \\ y_{d,l}^A &= i \varsigma_{d,l}, & y_u^A &= -i \varsigma_u^*. \end{aligned} \quad (8)$$

Then, the CP-conserving $A2HDM$ contains 10 real parameters: the three complex alignment constants $\varsigma_{u,d,l}$, the three scalar masses m_{A,H,H^\pm} , and the scalar mixing angle γ . We will assume that the light CP-even Higgs h is the SM-like Higgs with a mass of 125.09 GeV [25]. The other parameters have not yet been measured and they can be constrained by indirect phenomenological and theoretical arguments.

The presence of a charged Higgs is a signature of the model that allows some constraints coming from the phenomenology associated. In ref. [40] combined bounds on $\varsigma_{u,d,l}$ and m_{H^\pm} are obtained from: a) tau decays, $|\varsigma_l|/m_{H^\pm} \leq 0.40 \text{ GeV}^{-1}$, and b) a global fit to the tree leptonic and semi-leptonic decays of pseudoscalar mesons, $|\varsigma_u \varsigma_l^*|/m_{H^\pm}^2 \lesssim 0.01 \text{ GeV}^{-2}$ and $|\varsigma_d \varsigma_l^*|/m_{H^\pm}^2 \lesssim 0.1 \text{ GeV}^{-2}$. Bounds can be improved by looking at loop-induced processes, $Z \rightarrow b\bar{b}$, $B^0-\bar{B}^0$ and $K^0-\bar{K}^0$ mixing, and $\bar{B} \rightarrow X_s \gamma$, assuming that the dominant new-physics corrections to the observables are those generated by the charged scalar; then $|\varsigma_u| < 1.91$ for $m_{H^\pm} = 500 \text{ GeV}$ [40, 41].

Bounds on ς_d are more difficult to get from phenomenology so an upper bound as big as $|\varsigma_d| \leq 50$ can be used [41]. Studies of the radiative decays $\bar{B} \rightarrow X_{s,d} \gamma$, show that the combination $|\varsigma_u^* \varsigma_d|$ is strongly correlated with the mass of the scalar charged boson m_{H^\pm} , thus one find that $|\varsigma_u^* \varsigma_d| \leq 25$ for $m_{H^\pm} \in (100, 500) \text{ GeV}$ [40, 41]. More constraints on the $\varsigma_u-\varsigma_d$ plane can also be set from \bar{B} decays and are given in ref. [40, 41]

Recently, direct searches of light charged scalar Higgs in $t \rightarrow H^+ b$ decay in ATLAS and CMS [42] give an upper bound [43] on the combination $|\varsigma_u^* \varsigma_d|$ that excludes part of the allowed regions constrained by \bar{B} decays.

All these limits put constraints on the parameter space of the model. In this paper we only consider the ones that are related to the top physics.

3 V_R top coupling in the $A2HDM$

The most general Lorentz structure of the amplitude \mathcal{M}_{tbW} , for on-shell particles, in the $t(p) \rightarrow b(p')W^+(q)$ decay is:

$$\begin{aligned} \mathcal{M}_{tbW} &= -\frac{e}{\sin \theta_w \sqrt{2}} \epsilon^{\mu*} \times \\ &\quad \bar{u}_b(p') \left[\gamma_\mu (V_L P_L + V_R P_R) + \frac{i \sigma_{\mu\nu} q^\nu}{m_W} (g_L P_L + g_R P_R) \right] u_t(p), \end{aligned} \quad (9)$$

where the outgoing W^+ momentum, mass and polarization vector are $q = p - p'$, m_W and ϵ^μ , respectively. The couplings are all dimensionless; V_L and V_R parametrize the left and right vector couplings while g_L and g_R are the so called left and right anomalous tensor couplings, respectively.

In an effective Lagrangian approach these couplings arise as contributions of low energy non-renormalizable lagrangian terms, originated in a high energy theory. This approach assumes that the new physics spectrum is well above the electroweak (EW) energy scale [44–46].

The couplings V_R , g_R and g_L are zero at tree level within the SM, and V_L is given by the Kobayashi-Maskawa matrix element $V_L = V_{tb} \simeq 1$ [47]. The values of the anomalous tensor couplings at one loop have been calculated in ref. [27] for the SM, and in ref. [28] for a general $A2HDM$.

The SM contribution to V_R has been calculated in ref. [30]. There, the QCD one loop gluon exchange and the one loop contribution from the EW sector of the SM have been explicitly calculated. For the values of the standard masses and couplings given in [47], they are:

$$V_R(QCD) = 2.68 \times 10^{-3}, \quad V_R(EW) = (-0.015 + 8.92i) \times 10^{-5}. \quad (10)$$

Note that, as can be seen from ref. [30], the EW contribution to the real part of the V_R coupling from most of the EW diagrams is of the order of 10^{-5} but, due to accidental cancellations among them, the final result is two orders of magnitude smaller. In fact this real part, within the precision of our calculation and considering the uncertainties of the data used, is compatible with zero, at 10^{-7} precision.¹ The imaginary part, instead, remains of order 10^{-5} , and it is purely EW.

In the $2HDM$, the couplings structure of the tbW remains unchanged at tree level. However, at one loop, in addition to the usual particle contents of the SM, the three new neutral scalars h , H and A , and the new charged scalars H^\pm of the $2HDM$ may circulate in the internal lines of the loop and new contributions to the V_R coupling arise. The structure of the one loop diagrams contributing to the V_R top right-coupling is given in figure 1.

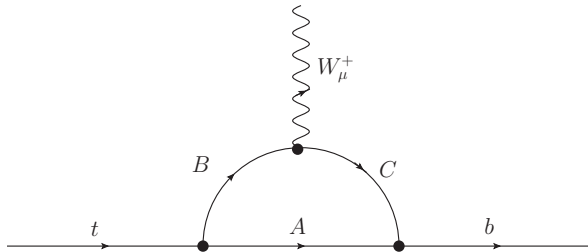


Figure 1: One-loop contributions to the V_R coupling in the $t \rightarrow bW^+$ vertex.

¹Notice that the result quoted here differs (even in sign) from the one of ref. [30]. As explained, this is so for two reasons: 1) the set of PDG values used here for the SM parameters is different and, 2) the accidental cancellation among diagrams makes the result very sensitive to these values, and consequently, the final result is not well determined and strongly depends on small changes on the SM masses and couplings within the experimental errors given in [47].

We denote each diagram by the label ABC according with the particles running in the loop. In table 1 we shown the 17 new diagrams to be considered, ordered by the position (A, B, or C) of the neutral scalars φ_i , where φ_i stands for one of the neutrals h , H and A in the diagram types from (1) to (3), while for diagrams types (4) to (7), φ_i runs only for the neutral scalar bosons h and H . It is important to notice that diagrams type (5) and (7) always have an imaginary part while, depending on the mass of the new scalar charged Higgs (H^\pm), diagrams type (2) may or may not develop it.

Type	Particles in the loop ABC	
(1)	$t \varphi_i H^-$	$\varphi_i = h, H, A$
(2)	$b H^+ \varphi_i$	
(3)	$\varphi_i t b$	
(4)	$t \varphi_i W^-$	$\varphi_i = h, H$
(5)	$b W^+ \varphi_i$	
(6)	$t \varphi_i G^-$	
(7)	$b G^+ \varphi_i$	

Table 1: Classification of the new the Feynman diagrams by the particles circulating in the loop.

Chirality imposes that all the contributions are proportional to the bottom mass and can be written as:

$$V_R^{ABC} = \alpha V_{tb} r_b I^{ABC}, \quad (11)$$

where $r_b = m_b/m_t$ and I^{ABC} is the Feynman integral corresponding to the given diagram. In appendix A we give the analytical expressions of all these integrals, for the diagrams shown in table 1.

The V_R coupling depends on the scalar mixing angle γ and on the alignment parameters ς_u and ς_d . The mass dependence is parametrized by the dimensionless variable $r_X = m_X/m_t$, where m_X is the mass of the particle X circulating in the loop. For the neutral scalar masses above the TeV scale, the Feynman integrals give negligible values when compared to the SM contributions. However, the V_R coupling is very sensitive to the new particles masses when they take lower values.

As in the SM, some of the diagrams are ultraviolet divergent, but we know that the total result must be finite. In appendix A it can be seen that the sum of diagrams (3), (6) and (7), to the SM diagrams $G^0 t b$, $t G^0 G^-$ and $b G^+ G^0$, respectively, cancel all the ultraviolet divergences and the total result is finite. This fact has been also used as a test of our analytical calculation².

We recover the SM expressions from the $A2HDM$ just by taking the $\varsigma_{u,d} \rightarrow 0$ limit and setting $\gamma = -\pi/2$, in such a way that the neutral scalar h has the same couplings as the SM Higgs boson. In that limit we explicitly checked that the contributions to the top right-coupling in the $A2HDM$ –diagrams type (3) to (7)– are identical to the corresponding ones in the SM obtained in ref. [30].

² The logarithmic terms in the expressions given in appendix A are the finite contributions coming from the sum of the divergent part of each of the diagrams evaluated.

4 Results

In this section we present the one loop corrections to the top right-coupling V_R in the $A2HDM$. As already stated, these corrections depend on the alignment parameters $\varsigma_{u,d}$, the scalar mixing angle γ and on the masses of the new particles: 2 neutrals scalars h and H , one axial A , and two charged scalars H^\pm . We write the alignment parameters as:

$$\varsigma_u = \rho_u e^{i\theta_u}, \quad \varsigma_d = \rho_d e^{i\theta_d}, \quad (12)$$

and we investigate separately the effects of modulus and phases on the top V_R right-coupling. In addition to the masses of the new particles we have five free parameters: $\rho_u, \rho_d, \theta_u, \theta_d$ and the mixing angle γ .

We chose different sets of values for the masses of the new neutral and charged scalar particles; the scenarios we consider are shown in table 2. The new scalar masses are taken to be of the order of 10^2 GeV [48, 49]. In the framework of $2HDM$ and under certain assumptions on its dominant decays, the charged scalar mass, m_{H^\pm} , is excluded to be below 85 GeV by LEP data [50]. Then, it can take values below the top quark mass, so that the decay $t \rightarrow bH^\pm$ is kinematically possible and therefore, type (2) diagrams may develop an absorptive part. These scenarios are called **(i)** in our paper and we fix for them the mass of the charged scalar, m_{H^\pm} , to be 150 GeV. For the other cases, where $m_{H^\pm} > m_t$, we take $m_{H^\pm} = 320$ GeV, as shown in table 2. In addition, for a CP conserving scalar potential [51] we have to impose that $m_h \leq m_H$. We define four different mass scenarios: two with three light neutral scalars (**I** and **Ii**) and two with h as the only light scalar (**II** and **IIi**). The other possible two, with the CP-odd scalar A being the lightest one, are disfavored by present LHC data [52, 53] and are not considered here.





Scalar mass scenarios (in GeV)					Type of line and color
	m_h	m_H	m_A	m_{H^\pm}	
I	125.09	173.21	150	320	
Ii	125.09	173.21	150	150	
II	125.09	866.05	866.05	320	
IIi	125.09	866.05	866.05	150	

Table 2: Different scalar mass scenarios taken for the analysis. As specified in the table, each scenario is identified by a different color and type of line in the plots.

The set of scenarios given in table 2 allows us to investigate the whole meaningful parameter space and to determine the regions where V_R strongly differs from the SM-EW prediction. In all scenarios the value of the heaviest (scalar or pseudoscalar particle) mass, 866.05 GeV, is fixed by setting $r_{heaviest} = (m_{heaviest})/m_t = 5$.

For our numerical analysis we define Q_V^{Im} as the ratio of the imaginary part of the

V_R coupling in the $A2HDM$ to the SM-EW:

$$Q_V^{\text{Im}} \equiv \frac{\text{Im}(V_R^{A2HDM})}{\text{Im}(V_R^{EW})}. \quad (13)$$

Regarding the analysis of the V_R real part, due to the uncertainty already commented in the SM-EW, we present the results for the $A2HDM$ in terms of $\text{Re}(V_R) = V_R^{\text{Re}}$.

For the four different mass scenarios defined in table 2, we study the V_R dependence on the four alignment parameters $\rho_{d,u}$, $\theta_{u,d}$, and on the scalar mixing angle γ . We show the results for conservative values of the modulus, *i.e.* for $\rho_{u,d} \sim 1$. Larger values of these modulus will certainly produce large deviations from the SM predictions but these values are disfavoured with present data [40, 41].

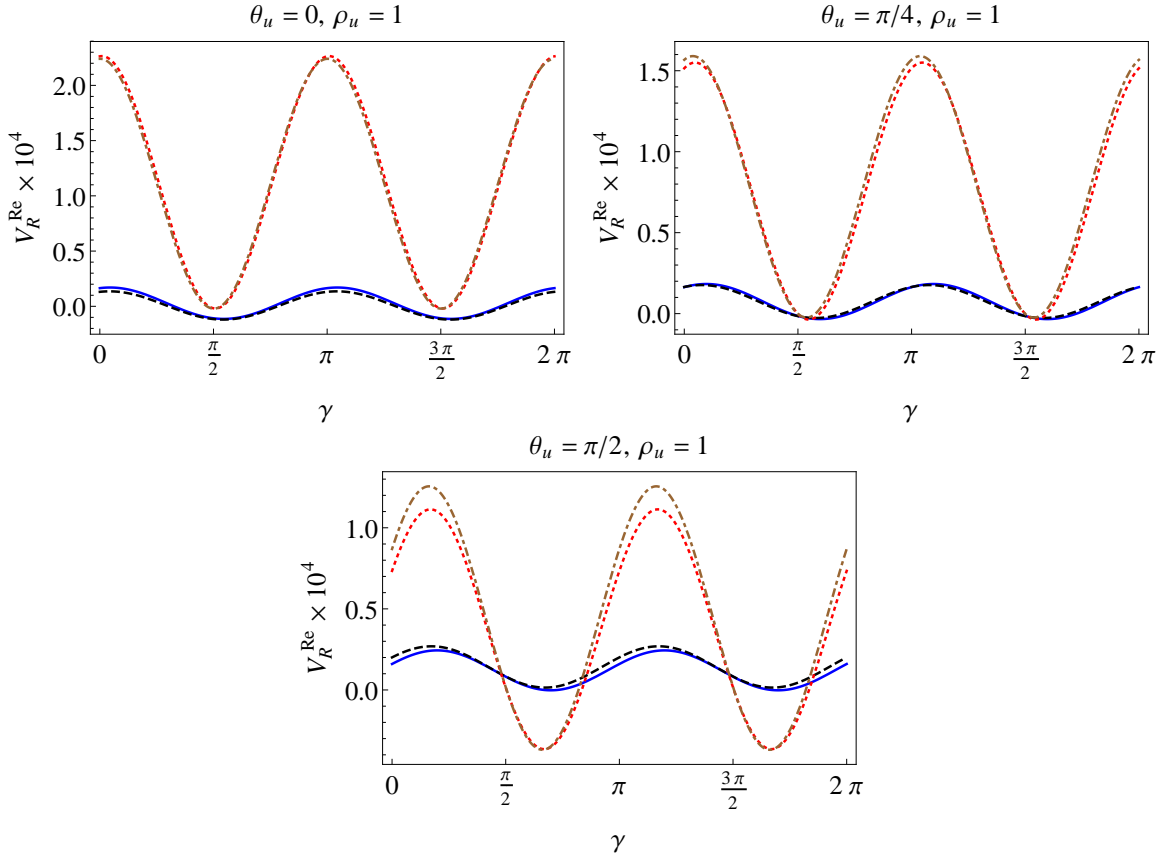


Figure 2: $V_R^{\text{Re}} = \text{Re}(V_R^{A2HDM})$, as a function of the γ scalar mixing angle, for different θ_u values and $\rho_{u,d} = 1$, $\theta_d = \pi/4$.

In figure 2 we show the dependence of V_R^{Re} on the γ mixing angle, for different values of the θ_u parameter, with $\rho_{u,d} = 1$ and fixing $\theta_d = \pi/4$. V_R^{Re} in the $A2HDM$ can be three orders of magnitude bigger than the SM-EW prediction for scenarios II and III, while it can be one order of magnitude larger for scenarios I and Ii. The behaviour with the γ parameter always exhibits the usual oscillating dependence. We checked

that these results do not depend crucially on the particular θ_d value chosen. Similar values -with a slight shift of the central values of the V_R coupling- are found when fixing $\theta_u = \pi/4$ and varying θ_d .

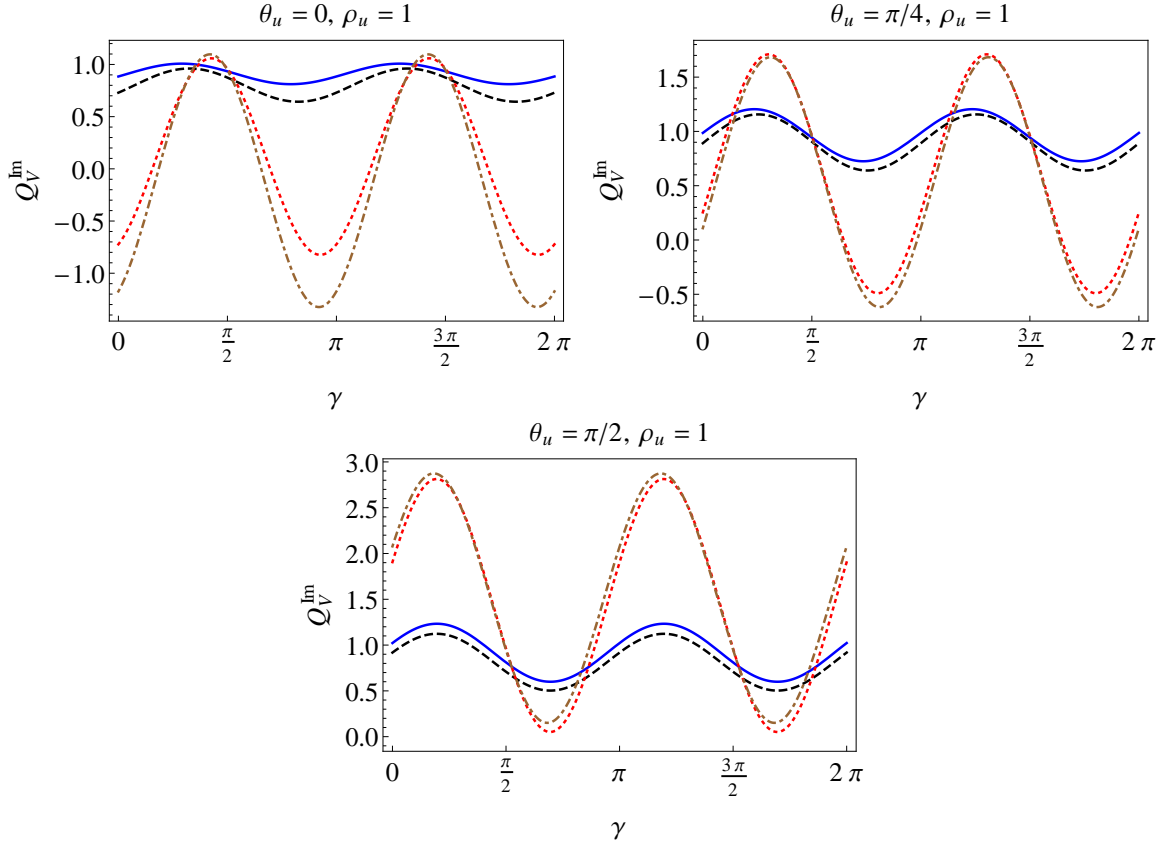


Figure 3: Q_V^{Im} , eq. (13) dependence with the γ scalar mixing angle, for different θ_u values and for $\rho_{u,d} = 1$, $\theta_d = \pi/4$.

In figure 3 we show the behaviour of Q_V^{Im} for the same set of parameters as given in figure 2. For $\rho_{u,d} = 1$, $\theta_d = \pi/4$, and θ_u given in the plots, it can be up to three times larger than the SM-EW value, as can be seen in the third plot of figure 3 (scenarios II and Ii). For scenarios I and Ii, the deviation from the SM-EW value is much smaller. The figures show the expected dependence of the observable with γ as a combination of $\sin \gamma$ and $\cos \gamma$. As in the real part of the coupling, the plots for $\text{Im}(V_R)$ present similar behaviour as the one shown in figure 3, with a small shift of their central values, when interchanging $\theta_u \leftrightarrow \theta_d$.

The V_R coupling is more sensitive to the values of ρ_u than to those of ρ_d . The last one may move over a wide range of values ($1 < \rho_d < 10$) without changing crucially the results. In the following we fix the values of the $\rho_d = 1$ and $\theta_d = \pi/4$ as a representative choice of these parameters and we study the dependence of V_R with the rest of the parameters of the model.

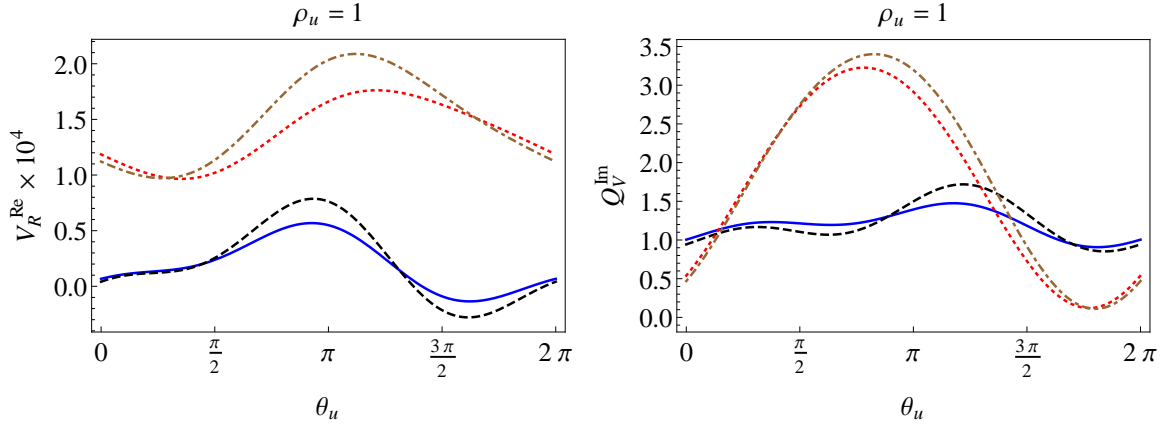


Figure 4: $V_R^{\text{Re}} = \text{Re}(V_R^{A2HDM})$ and Q_V^{Im} (eq. (13)) as function of the θ_u parameter, with $\gamma = \pi/4$, $\rho_d = 1$ and $\theta_d = \pi/4$.

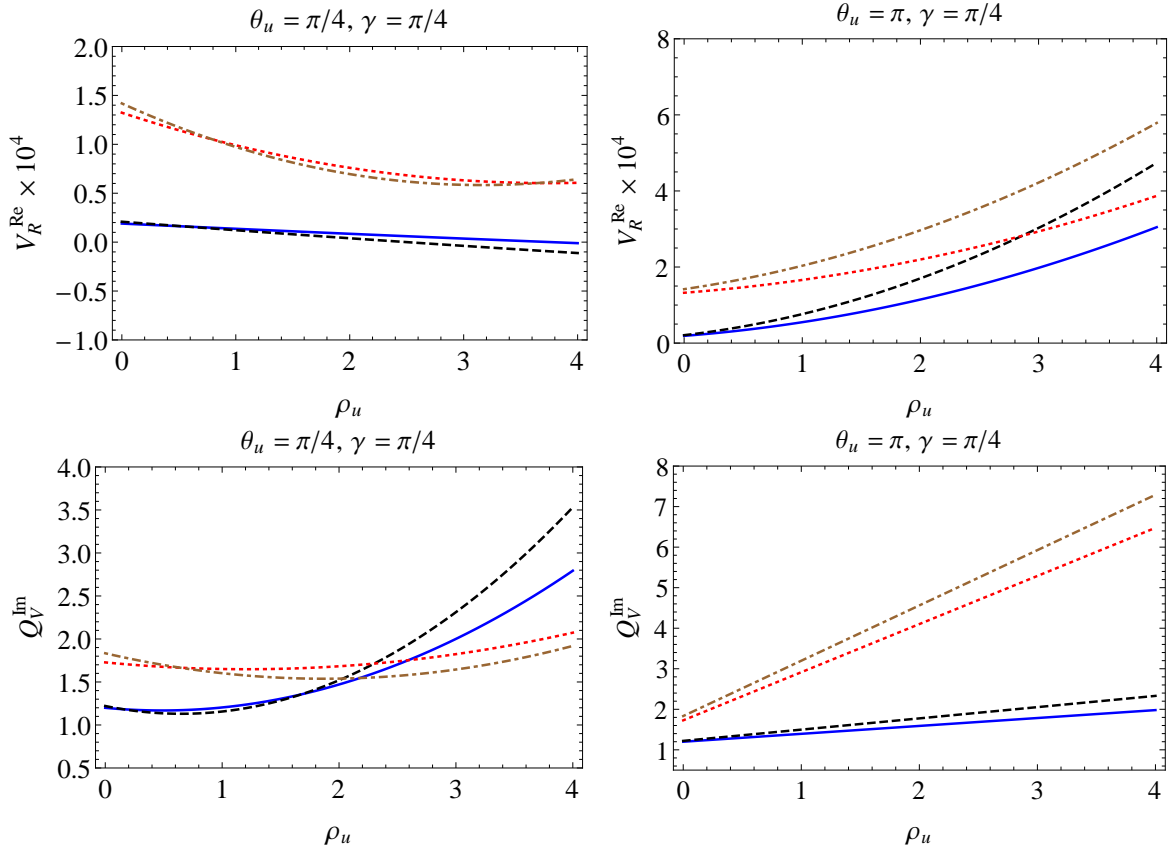


Figure 5: $V_R^{\text{Re}} = \text{Re}(V_R^{A2HDM})$ and Q_V^{Im} , eq. (13), as a function of ρ_u for values of θ_u given in the plots and for fixed values $\gamma = \pi/4$, $\rho_d = 1$ and $\theta_d = \pi/4$.

In figure 4 we show V_R (real and imaginary parts) as functions of the θ_u angle, for the scalar mixing angle $\gamma = \pi/4$. As seen there, the real part can be three (two) orders of magnitude bigger than the SM-EW one for scenarios II and IIi (I and Ii), while the

imaginary part can take values up to three times larger than the SM-EW prediction, for scenarios II and III.

In figure 5 we present the dependence of V_R with the coupling parameter ρ_u . The plots show that V_R^{Re} is three (two) orders of magnitude larger than the SM-EW value, for scenarios II and III (I and II). Besides, for large values of the ρ_u parameter, V_R^{Re} grows with ρ_u independently of the values of the other parameters of the model, such as γ and θ_u . A similar behaviour is found for the imaginary part of V_R , that can be a factor seven larger than the SM-EW one for large values of ρ_u .

Finally, we compute V_R for Type-I [54, 55] and Type-II [55, 56] $2HDM$ ³. In table 3 we show the $\varsigma_{u,d}$ values that reproduce the Type-I and Type-II models. These models have a discrete \mathcal{Z}_2 symmetry in order to avoid tree level FCNC.

Model	ς_d	ς_u
Type-I	$\cot \beta$	$\cot \beta$
Type-II	$-\tan \beta$	$\cot \beta$

Table 3: Values for $\varsigma_{u,d}$ that reproduce the Type-I and Type-II $2HDM$.

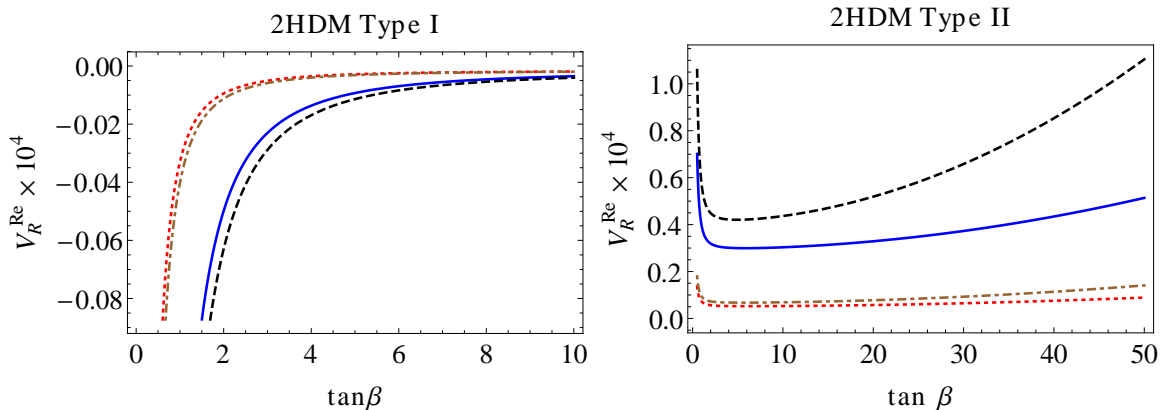


Figure 6: Type-I $2HDM$ prediction for V_R^{Re} (left) and Q_V^{Im} (right) as a function of $\tan \beta$, with $\gamma = -\pi/2$.

For Type-I and Type-II $2HDM$, we present the results as a function of $\tan \beta$, for the different mass scenarios considered. We work on the alignment limit, $\gamma = -\pi/2$, where the neutral scalar h has SM-like couplings to the photon and to the weak bosons. The results for the real part of V_R are shown in figure 6. For Type-I model, V_R takes values one order of magnitude larger than the SM-EW one, for $1 < \tan \beta < 4$ and for all mass scenarios; for $\tan \beta \gg 4$ it approaches the SM-EW value. Note that for Type-I $2HDM$ the Yukawa couplings go to zero in the large $\tan \beta$ limit. For Type-II model the value of V_R grows with $\tan \beta$, reaching values close to 10^{-4} (10^{-5}) for $\tan \beta \simeq 50$ in the mass scenarios I and II (II and III). We also find that, within these models, V_R^{Im} is very close to the SM-EW value and almost constant for the considered mass scenarios.

³See ref. [57] for a study of the values of the different top couplings in Type-I and Type-II $2HDM$.

5 Conclusions

We computed the one-loop contribution to V_R in the $A2HDM$. In the SM, accidental cancellation among the one loop EW parts results in values for V_R^{Re} two orders of magnitude smaller than expected from each diagram. This cancellation does not take place in the $A2HDM$. Then, depending on the values of the parameters of the model, the magnitude of V_R^{Re} can be three orders of magnitude larger than the SM-EW prediction (i.e. close to 10^{-4}) and close to the leading QCD contribution. V_R^{Im} can be one order of magnitude larger than the SM prediction for $\rho_{u,d} > 4$ but, for $\rho_{u,d} \sim 1$, its magnitude is only a few times larger. For Type-II (Type-I) $2HDM$, V_R^{Re} can grow up to two (one) orders of magnitude with respect the SM-EW value, for $\tan \beta \approx 10$ and depending of the mass scenarios considered, while the imaginary part remains basically of the same order as in the SM-EW. As it is shown in our previous work [30], new observables for the LHC and next generation colliders can provide a direct measurement of the right top coupling V_R .

6 Acknowledgments

This work has been supported, in part, by the Ministerio de Economía y Competitividad (MINECO), Spain, under grants FPA2014-54459-P and SEV-2014-0398; by Generalitat Valenciana, Spain, under grant PROMETEOII2014-087. G.A.G-S. acknowledges the support of CSIC and Pedeciba, Uruguay. C.A. acknowledges the support by the Spanish Government and ERDF funds from the EU Commission [Grant No. FPA2014-53631-C2-1-P] and by CONICYT Fellowship ‘‘Becas Chile’’ Grant No. 74150052. R.M. also thanks to COLCIENCIAS.

Appendix A $A2HDM$ contribution to V_R

Following the notation of ref. [30], we define

$$A_a = x^2 [((y-1)r_b^2 + 1)y - r_w^2(y-1)] - r_a^2(x-1), \quad (14)$$

$$\tilde{A}_a = A_a(r_w \rightarrow r_{H^+}), \quad (15)$$

$$B_a = x \{ [(x(y-1) + 1)r_b^2 + x - 1]y - r_a^2(y-1) \} \\ - r_w^2(x-1)[x(y-1) + 1], \quad (16)$$

$$\tilde{B}_a = B_a(r_w \rightarrow r_{H^+}), \quad (17)$$

$$C_a = (x-1)(xy-1)r_b^2 - r_w^2(x-1)x(y-1) + r_a^2xy + x(y-1)(xy-1), \quad (18)$$

with

$$r_x \equiv \frac{m_x}{m_t}, \quad (19)$$

and

$$\begin{aligned} y_d^H &= \cos \gamma + \sin \gamma \varsigma_d, & y_u^H &= \cos \gamma + \sin \gamma \varsigma_u^*, \\ y_d^h &= -\sin \gamma + \cos \gamma \varsigma_d, & y_u^h &= -\sin \gamma + \cos \gamma \varsigma_u^*, \\ y_d^A &= i \varsigma_d, & y_u^A &= -i \varsigma_u^*. \end{aligned} \quad (20)$$

Then, we have the following expressions for the new contributions, listed in table 1:

- Type (1) diagrams.

$$\begin{aligned}
I^{tHH^-} + I^{thH^-} + I^{tAH^-} &= \frac{1}{16\pi s_w^2 r_w^2} \times \\
&\int_0^1 dx \int_0^1 dy x \left\{ \varsigma_d \left[y_u^H \sin \gamma \ln \frac{\tilde{A}_H}{\tilde{A}_A} + y_u^h \cos \gamma \ln \frac{\tilde{A}_h}{\tilde{A}_A} \right] \right. \\
&\left. + yx \left[\frac{v_R^{uHH^+}}{\tilde{A}_H} \sin \gamma + \frac{v_R^{uhH^-}}{\tilde{A}_h} \cos \gamma - i \frac{v_R^{uAH^-}}{\tilde{A}_A} \right] \right\}, \tag{21}
\end{aligned}$$

with

$$\begin{aligned}
v_R^{u\varphi_i H^-} &= -y_u^{\varphi_i} \{ \varsigma_d [r_b^2(1-y)x + (1-x)] - \varsigma_u \} \\
&+ y_u^{\varphi_i^*} [\varsigma_u(1-xy) - \varsigma_d], \quad \varphi_i = h, H, A. \tag{22}
\end{aligned}$$

- Type (2) diagrams.

$$\begin{aligned}
I^{bH^+H} + I^{bH^+h} + I^{bH^+A} &= -\frac{1}{16\pi s_w^2 r_w^2} \times \\
&\int_0^1 dx \int_0^1 dy x \left\{ \varsigma_u \left[y_d^{H^*} \sin \gamma \ln \frac{\tilde{B}_H}{\tilde{B}_A} + y_d^{h^*} \cos \gamma \ln \frac{\tilde{B}_h}{\tilde{B}_A} \right] \right. \\
&\left. + yx \left[\frac{v_R^{dH^+H}}{\tilde{B}_H} \sin \gamma + \frac{v_R^{dH^+h}}{\tilde{B}_h} \cos \gamma - i \frac{v_R^{dH^+A}}{\tilde{B}_A} \right] \right\}, \tag{23}
\end{aligned}$$

with

$$\begin{aligned}
v_R^{dH^+\varphi_i} &= -y_d^{\varphi_i} r_b^2 [\varsigma_d(1-xy) - \varsigma_u] \\
&+ y_d^{\varphi_i^*} \{ \varsigma_u [(1-y)x r_b^2 + (1-x)] - \varsigma_d r_b^2 \}, \quad \varphi_i = h, H, A. \tag{24}
\end{aligned}$$

- Type (3) diagrams.

$$\begin{aligned}
I^{G^0tb} + I^{Htb} + I^{htb} + I^{Atb} &= \frac{1}{16\pi s_w^2} \times \\
&\int_0^1 dx \int_0^1 dy x \left\{ x(1-x)(1-y) \left[-\frac{1}{C_Z} + \frac{y_d^{H^*} y_u^H}{C_H} + \frac{y_d^{h^*} y_u^h}{C_h} + \frac{y_d^{A^*} y_u^A}{C_A} \right] \right. \\
&\left. - \frac{1}{r_w^2} \left[y_d^{H^*} y_u^H \ln \frac{C_H}{C_Z} + y_d^{h^*} y_u^h \ln \frac{C_h}{C_Z} + y_d^{A^*} y_u^A \ln \frac{C_A}{C_Z} \right] \right\}. \tag{25}
\end{aligned}$$

- Type (6) diagrams.

$$\begin{aligned}
I^{tG^0G^-} + I^{tHG^-} + I^{thG^-} &= \frac{1}{16\pi s_w^2 r_w^2} \times \\
&\int_0^1 dx \int_0^1 dy x \left\{ x^2 y \left[-\frac{1+y-r_b^2(1-y)}{A_Z} + \frac{(r_b^2(y-1)+1)y_u^H - y y_u^{H^*}}{A_H} \cos \gamma \right. \right. \\
&\left. \left. - \frac{(r_b^2(y-1)+1)y_u^h - y y_u^{h^*}}{A_h} \sin \gamma \right] \right. \\
&\left. + y_u^H \cos \gamma \ln \frac{A_H}{A_Z} - y_u^h \sin \gamma \ln \frac{A_h}{A_Z} \right\}. \tag{26}
\end{aligned}$$

- Type (7) diagrams.

$$\begin{aligned}
I^{bG^+G^0} + I^{bG^+H} + I^{bG^+h} &= \frac{1}{16\pi s_w^2 r_w^2} \times \\
&\int_0^1 dx \int_0^1 dy x \left\{ xy \left[\frac{1-x-r_b^2(1-x(1-2y))}{B_Z} \right. \right. \\
&+ \frac{(r_b^2((y-1)x+1)+x-1)y_d^{H^*} - xy r_b^2 y_d^H}{B_H} \cos \gamma \\
&\left. \left. - \frac{(r_b^2((y-1)x+1)+x-1)y_d^{h^*} - xy r_b^2 y_d^h}{B_h} \sin \gamma \right] \right. \\
&\left. + y_d^{H^*} \cos \gamma \ln \frac{B_H}{B_Z} - y_d^{h^*} \sin \gamma \ln \frac{B_h}{B_Z} \right\}. \tag{27}
\end{aligned}$$

The contribution from type (4), $\{t\varphi_i W\}$, and type (5), $\{bW\varphi_i\}$, diagrams ($\varphi_i = h, H$) is zero as in the SM:

$$V_R^{t\varphi_i W^-} = V_R^{bW^+\varphi_i} = 0, \quad \varphi_i = h, H. \tag{28}$$

Notice that in the limit $\varsigma_{u,d} \rightarrow 0$, and fixing $\gamma = -\pi/2$ to identifying h with the standard Higgs, we recover the SM result [30].

References

- [1] M. Selvaggi, *Perspectives for Top quark physics at High-Luminosity LHC*, *PoS TOP2015* (2016) 054, [arXiv:1512.04807].
- [2] W. Barletta, M. Battaglia, M. Klute, M. Mangano, S. Prestemon, L. Rossi, and P. Skands, *Working Group Report: Hadron Colliders*, in *Proceedings, Community Summer Study 2013: Snowmass on the Mississippi (CSS2013): Minneapolis, MN, USA, July 29-August 6, 2013*, 2013. arXiv:1310.0290.
- [3] **CDF Collaboration** Collaboration, F. Abe et al., *Observation of top quark production in $\bar{p}p$ collisions*, *Phys. Rev. Lett.* **74** (1995) 2626–2631, [hep-ex/9503002].
- [4] **D0 Collaboration** Collaboration, S. Abachi et al., *Observation of the top quark*, *Phys. Rev. Lett.* **74** (1995) 2632–2637, [hep-ex/9503003].
- [5] C. Deterre, *W helicity and constraints on the Wtb vertex at the Tevatron*, *Nuovo Cim.* **C035N3** (2012) 125–129, [arXiv:1203.6802].
- [6] **D0 Collaboration** Collaboration, V. M. Abazov et al., *Search for anomalous Wtb couplings in single top quark production in $p\bar{p}$ collisions at $\sqrt{s} = 1.96$ TeV*, *Phys. Lett. B* **708** (2012) 21–26, [arXiv:1110.4592].

- [7] **D0** Collaboration, V. M. Abazov et al., *Search for anomalous Wtb couplings in single top quark production*, *Phys. Rev. Lett.* **101** (2008) 221801, [arXiv:0807.1692].
- [8] W. Bernreuther, *Top quark physics at the LHC*, *J. Phys. G* **35** (2008) 083001, [arXiv:0805.1333].
- [9] D. Bardhan, G. Bhattacharyya, D. Ghosh, M. Patra, and S. Raychaudhuri, *Detailed analysis of flavor-changing decays of top quarks as a probe of new physics at the LHC*, *Phys. Rev.* **D94** (2016), no. 1 015026, [arXiv:1601.04165].
- [10] W. Bernreuther, D. Heisler, and Z.-G. Si, *A set of top quark spin correlation and polarization observables for the LHC: Standard Model predictions and new physics contributions*, *JHEP* **12** (2015) 026, [arXiv:1508.05271].
- [11] F.-P. Schilling, *Top Quark Physics at the LHC: A Review of the First Two Years*, *Int. J. Mod. Phys.* **A27** (2012) 1230016, [arXiv:1206.4484].
- [12] C. Bernardo, N. F. Castro, M. C. N. Fiolhais, H. Gonçalves, A. G. C. Guerra, M. Oliveira, and A. Onofre, *Studying the Wtb vertex structure using recent LHC results*, *Phys. Rev.* **D90** (2014), no. 11 113007, [arXiv:1408.7063].
- [13] R. Hawkings, *Top quark physics at the LHC*, *Comptes Rendus Physique* **16** (2015) 424–434.
- [14] M. Cristinziani and M. Mulders, *Top-quark physics at the Large Hadron Collider*, arXiv:1606.00327.
- [15] **ATLAS** Collaboration, D. Calvet, *Search for New Physics with Top quarks in ATLAS at 8 TeV ($t\bar{b}$, $t\bar{t}$, vector-like quarks)*, in *Proceedings, 20th International Conference on Particles and Nuclei (PANIC 14): Hamburg, Germany, August 24-29, 2014*, pp. 579–582, 2014.
- [16] **ATLAS, CMS** Collaboration, D. Pagano, *Measurements of new physics in top quark decay at LHC*, *J. Phys. Conf. Ser.* **452** (2013), no. 1 012011.
- [17] R. Gaitan, E. A. Garces, J. H. M. de Oca, and R. Martinez, *Top quark Chromoelectric and Chromomagnetic Dipole Moments in a Two Higgs Doublet Model with CP violation*, *Phys. Rev.* **D92** (2015), no. 9 094025, [arXiv:1505.04168].
- [18] F. del Aguila and J. Aguilar-Saavedra, *Precise determination of the Wtb couplings at CERN LHC*, *Phys.Rev.* **D67** (2003) 014009, [hep-ph/0208171].
- [19] J. Aguilar-Saavedra and J. Bernabéu, *W polarisation beyond helicity fractions in top quark decays*, *Nucl. Phys. B* **840** (2010) 349–378, [arXiv:1005.5382].
- [20] J. Drobnak, S. Fajfer, and J. F. Kamenik, *New physics in $t \rightarrow bW$ decay at next-to-leading order in QCD*, *Phys. Rev.* **D82** (2010) 114008, [arXiv:1010.2402].

- [21] S. D. Rindani and P. Sharma, *Probing anomalous tbW couplings in single-top production using top polarization at the Large Hadron Collider*, *JHEP* **1111** (2011) 082, [[arXiv:1107.2597](#)].
- [22] A. V. Prasath, R. M. Godbole, and S. D. Rindani, *Longitudinal top polarisation measurement and anomalous Wtb coupling*, *Eur. Phys. J.* **C75** (2015), no. 9 402, [[arXiv:1405.1264](#)].
- [23] Q.-H. Cao, B. Yan, J.-H. Yu, and C. Zhang, *A General Analysis of Wtb anomalous Couplings*, [arXiv:1504.03785](#).
- [24] Z. Hioki and K. Ohkuma, *Full analysis of general non-standard tbw couplings*, *Physics Letters B* **752** (2016) 128 – 130.
- [25] C. Patrignani, *Review of Particle Physics*, *Chin. Phys.* **C40** (2016), no. 10 100001.
- [26] M. Moreno Llácer, *Search for CP violation in single top quark events with the ATLAS detector at LHC*. PhD thesis, Valencia U., IFIC, 2014.
- [27] G. A. González-Sprinberg, R. Martinez, and J. Vidal, *Top quark tensor couplings*, *JHEP* **07** (2011) 094, [[arXiv:1105.5601](#)]. [Erratum: *JHEP*05,117(2013)].
- [28] L. Duarte, G. A. González-Sprinberg, and J. Vidal, *Top quark anomalous tensor couplings in the two-Higgs-doublet models*, *JHEP* **1311** (2013) 114, [[arXiv:1308.3652](#)].
- [29] W. Bernreuther, P. Gonzalez, and M. Wiebusch, *The Top Quark Decay Vertex in Standard Model Extensions*, *Eur. Phys. J. C* **60** (2009) 197–211, [[arXiv:0812.1643](#)].
- [30] G. A. González-Sprinberg and J. Vidal, *The top quark right coupling in the tbW -vertex*, *Eur. Phys. J.* **C75** (2015), no. 12 615, [[arXiv:1510.02153](#)].
- [31] B. Lampe, *Forward - backward asymmetry in top quark semileptonic decay*, *Nucl.Phys.* **B454** (1995) 506–526.
- [32] J. Aguilar-Saavedra, J. Carvalho, N. F. Castro, F. Veloso, and A. Onofre, *Probing anomalous Wtb couplings in top pair decays*, *Eur.Phys.J.* **C50** (2007) 519–533, [[hep-ph/0605190](#)].
- [33] B. Grzadkowski and Z. Hioki, *New hints for testing anomalous top quark interactions at future linear colliders*, *Phys.Lett.* **B476** (2000) 87–94, [[hep-ph/9911505](#)].
- [34] R. M. Godbole, S. D. Rindani, and R. K. Singh, *Lepton distribution as a probe of new physics in production and decay of the t quark and its polarization*, *JHEP* **0612** (2006) 021, [[hep-ph/0605100](#)].

- [35] T. Stelzer and S. Willenbrock, *Spin correlation in top quark production at hadron colliders*, *Phys.Lett.* **B374** (1996) 169–172, [[hep-ph/9512292](#)].
- [36] G. Mahlon and S. J. Parke, *Angular correlations in top quark pair production and decay at hadron colliders*, *Phys.Rev.* **D53** (1996) 4886–4896, [[hep-ph/9512264](#)].
- [37] A. Pich and P. Tuzon, *Yukawa Alignment in the Two-Higgs-Doublet Model*, *Phys. Rev. D* **80** (2009) 091702, [[arXiv:0908.1554](#)].
- [38] T. D. Lee, *A Theory of Spontaneous T Violation*, *Phys. Rev.* **D8** (1973) 1226–1239.
- [39] G. Branco, P. Ferreira, L. Lavoura, M. Rebelo, M. Sher, et al., *Theory and phenomenology of two-Higgs-doublet models*, *Phys. Rept.* **516** (2012) 1–102, [[arXiv:1106.0034](#)].
- [40] M. Jung, A. Pich, and P. Tuzon, *Charged-Higgs phenomenology in the Aligned two-Higgs-doublet model*, *JHEP* **1011** (2010) 003, [[arXiv:1006.0470](#)].
- [41] M. Jung, X.-Q. Li, and A. Pich, *Exclusive radiative B-meson decays within the aligned two-Higgs-doublet model*, *JHEP* **1210** (2012) 063, [[arXiv:1208.1251](#)].
- [42] **ATLAS, CMS Collaboration**, D. Chakraborty, *Charged Higgs boson searches at the LHC*, *Nucl. Part. Phys. Proc.* **260** (2015) 216–220.
- [43] A. Celis, V. Ilisie, and A. Pich, *Towards a general analysis of LHC data within two-Higgs-doublet models*, *JHEP* **12** (2013) 095, [[arXiv:1310.7941](#)].
- [44] W. Buchmuller and D. Wyler, *Effective Lagrangian Analysis of New Interactions and Flavor Conservation*, *Nucl. Phys. B* **268** (1986) 621.
- [45] J. Aguilar-Saavedra, *A Minimal set of top anomalous couplings*, *Nucl. Phys. B* **812** (2009) 181–204, [[arXiv:0811.3842](#)].
- [46] G. L. Kane, G. Ladinsky, and C. Yuan, *Using the Top Quark for Testing Standard Model Polarization and CP Predictions*, *Phys. Rev. D* **45** (1992) 124–141.
- [47] **Particle Data Group Collaboration**, K. Olive et al., *Review of Particle Physics*, *Chin.Phys.* **C38** (2014) 090001.
- [48] **CDF Collaboration** Collaboration, T. Aaltonen et al., *Search for a Higgs Boson in the Diphoton Final State in $p\bar{p}$ Collisions at $\sqrt{s} = 1.96$ TeV*, *Phys. Rev. Lett.* **108** (2012) 011801, [[arXiv:1109.4427](#)].
- [49] **D0 Collaboration** Collaboration, V. Abazov et al., *Search for the standard model and a fermiophobic Higgs boson in diphoton final states*, *Phys. Rev. Lett.* **107** (2011) 151801, [[arXiv:1107.4587](#)].

- [50] **LEP, DELPHI, OPAL, ALEPH, L3** Collaboration, G. Abbiendi et al., *Search for Charged Higgs bosons: Combined Results Using LEP Data*, *Eur. Phys. J. C* **73** (2013) 2463, [[arXiv:1301.6065](#)].
- [51] J. F. Gunion, H. E. Haber, G. L. Kane, and S. Dawson, *THE HIGGS HUNTER'S GUIDE*, *Front. Phys.* **80** (2000) 1–448.
- [52] **CMS** Collaboration, V. Khachatryan et al., *Search for a low-mass pseudoscalar Higgs boson produced in association with a $b\bar{b}$ pair in pp collisions at $\sqrt{s} = 8$ TeV*, *Phys. Lett. B* **758** (2016) 296–320, [[arXiv:1511.03610](#)].
- [53] A. Celis, V. Ilisie, and A. Pich, *LHC constraints on two-Higgs doublet models*, *JHEP* **1307** (2013) 053, [[arXiv:1302.4022](#)].
- [54] H. Haber, G. L. Kane, and T. Sterling, *The Fermion Mass Scale and Possible Effects of Higgs Bosons on Experimental Observables*, *Nucl.Phys. B* **161** (1979) 493.
- [55] L. J. Hall and M. B. Wise, *Flavor changing Higgs boson couplings*, *Nucl.Phys. B* **187** (1981) 397.
- [56] J. F. Donoghue and L. F. Li, *Properties of Charged Higgs Bosons*, *Phys.Rev. D* **19** (1979) 945.
- [57] A. Arhrib and A. Jueid, *tbW Anomalous Couplings in the Two Higgs Doublet Model*, *JHEP* **08** (2016) 082, [[arXiv:1606.05270](#)].